INTERNATIONAL JOURNAL FOR NUMERICAL METHODS IN FLUIDS, VOL. 10, 569–589 (1990)

# FLUID FLOW IN CURVED DUCTS

S. JAYANTI,* G. F. HEWITT† AND J. R. KIGHTLEY‡
*Harwell Laboratory, UKAEA, Oxfordshire, OX11 ORA, U.K.*

SUMMARY

The advent of standard algorithms for the numerical solution of partial differential equations has given researchers a new tool for fluid flow calculations. In this paper, single-phase flow in curved ducts is numerically simulated by imposing a spatially varying centrifugal force on a fluid flowing in a straight tube. The resulting set of partial differential equations is solved using the HARWELL-FLOW3D computer program. Comparison with other numerical and experimental results shows that this simplified formulation gives accurate results. The model neglects certain geometric terms of the order $d/D$, the duct-to-coil diameter ratio. The effect of these terms is investigated by considering the flow in a 90° bend for large $d/D$. It is shown that while there may be significant error in the prediction of the local variables for large $d/D$, the circumference-averaged quantities are well predicted.

KEY WORDS Numerical simulation Centrifugal force Finite difference method Laminar flow Heat transfer Coils Bends

## 1. INTRODUCTION

Fluid flow in bends and coils is encountered in many industrial situations. An important feature of such flow is the presence of secondary flow in a plane normal to the axial flow direction. This has the effect of increasing the average pressure drop and heat transfer coefficient as compared to straight tubes. The prediction of these quantities is important for the optimum design of industrial equipment, and this need is reflected in many studies conducted over the past 60 years.[1–10]

Traditionally, engineers and scientists have used theoretical and experimental techniques for the study of fluid flow. However, both techniques have their shortcomings and have only limited application. With the increased complexity of design equipment, coupled with the parallel development of computers and standard numerical algorithms, the trend nowadays is to use numerical techniques to solve a governing set of partial (or ordinary) differential equations; the role of experimental techniques is increasingly being relegated to that of generating data for the development and validation of numerical models.

However, the application of numerical techniques to practical flow situations is fraught with problems, arising partly from the physical complexity of the flow (e.g. turbulence) and partly from the geometrical complexity of the solution domain. For the study of fluid flow in bends and coils we encounter both sources of problems, but the motivation for this study comes from those arising from geometrical complexity. The numerical solution of flow in curved ducts often

*Post-graduate student, Imperial College, London, U.K.
†Thermal Hydraulics Division, Harwell Laboratory.
‡Computer Science and Systems Division, Harwell Laboratory.

0271–2091/90/050569–21$10.50

*Received December 1988*
*Revised June 1989*

requires the use of a general non-orthogonal grid in which irregular-shaped control volumes are used to fit the physical flow domain. While the solution of transport equations in simple orthogonal co-ordinate systems on regular grids is well understood and is relatively straightforward, the equations on general non-orthogonal girds are much more complicated and are difficult to code. Moreover, they usually contain cross-derivatives in pressure and other variables which give rise to major computational problems. While these problems can be overcome, this can only be done by resorting to sophisticated codes and techniques[11,12] which are beyond the reach and comprehension of the design engineer.

With this in mind, we present a simplified formulation for the calculation of the flow field in coils and bends: the flow is treated as that in a straight tube in which each fluid element is subject to a centrifugal force. This straight-tube formulation of the problem permits the use of simple co-ordinate systems, such as a Cartesian (cylindrical) co-ordinate system for a duct of rectangular (circular) cross-section. We illustrate its validity in simulating laminar, turbulent and buoyant flow in helical coils.

## 2. MATHEMATICAL FORMULATION OF THE PROBLEM

Fluid flow in a helical coil is generally treated in a toroidal co-ordinate system[7-9] which is not available as a standard option in many general-purpose programs for calculating three-dimensional flows. While it is possible in principle to convert a cylindrical co-ordinate system into a toroidal co-ordinate system by adding the extra terms as source terms, it is difficult because of the amount of coding involved. In view of this, the problem of flow in a curved duct is reformulated in a simpler manner by treating it as a flow in a straight duct in which each fluid element is subject to a centrifugal force given by $F_c = \rho u^2/R'$, where $u$ is the axial velocity of the fluid element and $R'$ is the local radius of curvature of the path taken by the fluid element had it been flowing in a helical coil (the notation used is given in Appendix I). As shown in Appendix II, the addition of $F_c$ as a body force correctly models the acceleration experienced by a fluid element moving in a curved path; however, the model neglects certain geometrical terms which are of the order of $d/D$ or higher. As will be shown later, this approximation introduces an error in predicting local variables for sharp bends, but the circumference-averaged quantities are well predicted. We note that this straight-tube formulation makes it possible to specify the problem of flow in curved pipes using a Cartesian or cylindrical co-ordinate system as shown in Figure 1. The centrifugal force is resolved along the three axes and is added to the respective momentum equations as a source term. Thus the mathematical model of steady state flow in a helical coil of circular cross-section is as follows:

continuity,

$$\nabla \cdot (\rho \mathbf{u}) = 0; \tag{1}$$

$x$-momentum (axial direction),

$$\nabla \cdot (\rho u u) - \nabla \cdot (\mu \nabla u) = -\frac{\partial p}{\partial x}; \tag{2}$$

$r$-momentum (radial direction),

$$\nabla \cdot (\rho u v) - \nabla \cdot (\mu \nabla v) = -\frac{\partial p}{\partial r} + \frac{\rho u^2}{R'} \cos\theta; \tag{3}$$

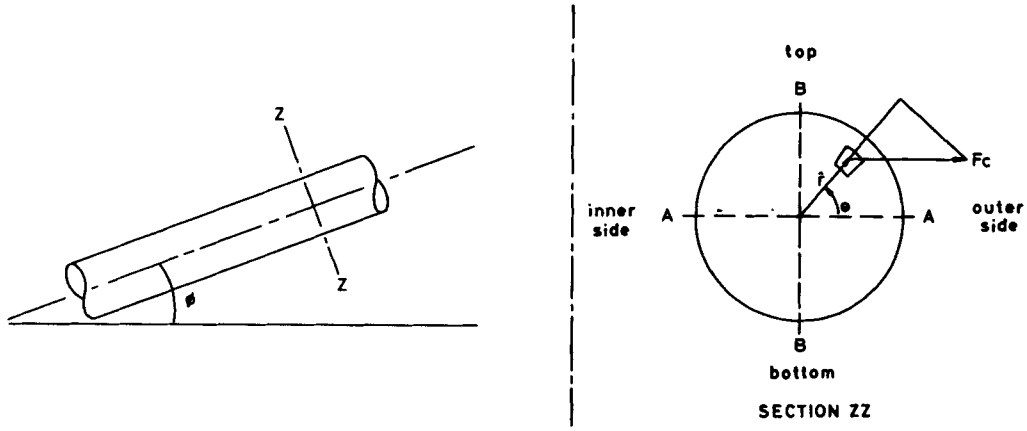


Figure 1. Straight-tube formulation: simulation of flow in a helical coil by imposing a centrifugal force on fluid flowing in a straight tube inclined at the helix angle $\phi$

$\theta$-momentum (circumferential direction),

$$\nabla\cdot(\rho u w)-\nabla\cdot(\mu\nabla w)=-\frac{1}{r}\frac{\partial p}{\partial\theta}-\frac{\rho u^2}{R'}\sin\theta; \tag{4}$$

energy,

$$\nabla\cdot(\rho\mathbf{u}T)-\nabla\cdot\left(\frac{\lambda}{C_p}\nabla T\right)=0. \tag{5}$$

These equations are solved as a set of elliptical partial differential equations with constant physical properties, i.e. $\rho$, $\mu$, $C_p$ and $\lambda$ are specified. The following boundary conditions are used:

inlet, plug velocity and temperature profiles;
outlet, fully developed flow, i.e. $\partial(\ )/\partial x=0$;
wall, no-slip boundary condition for the momentum equation, i.e. $u=v=w=0$ at $r=r_0$.

For the energy equation, either a constant heat flux ($-q''/\kappa$) or a constant wall temperature ($T_w=T_0$) is applied as boundary condition.

For turbulent flow calculations the standard $k$–$\varepsilon$ model[13] is used and a log-layer is imposed at the wall.[12] The addition of the centrifugal force term $F_c$ in the momentum equations introduces extra terms in the $k$–$\varepsilon$ model. These terms are derived in Appendix III. In cylindrical co-ordinates the additional term in the $k$-equation is given by

$$\frac{2\rho\bar{u}}{R'}(\overline{u'v'}\cos\theta-\overline{u'w'}\sin\theta),$$

where $u'$, $v'$ and $w'$ are the fluctuating velocity components and the overbar indicates time averaging. Following the formulation of the $k$–$\varepsilon$ model, $\overline{u'v'}$ and $\overline{u'w'}$ are evaluated by

$$\overline{u_i'u_j'}\simeq-\nu_t\left(\frac{\partial\bar{u}_i}{\partial x_j}+\frac{\partial\bar{u}_j}{\partial x_i}\right).$$

The extra terms in the $\varepsilon$-equation are derived in a manner analogous to that of the buoyancy term,[13] namely by multiplying the extra term in the $k$-equation by $\varepsilon/k$. Thus the following source term is added to the $\varepsilon$-equation:

$$\frac{2\rho\tilde{u}}{R'}\frac{\varepsilon}{k}(\overline{u'v'}\cos\theta - \overline{u'w'}\sin\theta).$$

The effect of buoyancy is considered in some cases. A Boussinesq approximation[14] is used; that is, an extra body force due to density variations caused by temperature differences of the form $\rho_{\text{ref}}\mathbf{g}\beta(T-T_{\text{ref}})$ is added to the appropriate momentum equations.

## 3. NUMERICAL SOLUTION PROCEDURE

The above set of partial differential equations was solved using the HARWELL-FLOW3D computer program,[12] which predicts flows in complex three-dimensional geometries. The program uses a finite difference method on a general non-orthogonal body-fitted grid. In contrast with most fluid flow algorithms, a non-staggered grid is used with velocity components in fixed directions. A modified and three-dimensional version of the Rhie and Chow algorithm[15] is used to suppress difficulties due to chequerboard oscillations in pressure and velocity traditionally associated with naive use of non-staggered grids. The program has a polyalgorithmic structure, whereby options are available for the user to specify different discretization schemes, solution algorithms and linear algebra solvers. Special effort has been expended in vectorizing the code for efficient running on the range of CRAY computers.

In the present problem the SIMPLEC[16] pressure correction algorithm was used to determine the velocity and pressure fields. It was found that the use of PISO[17] did not improve the convergence characteristics. The hybrid differencing scheme[18] was used to estimate convective fluxes. Other differencing schemes such as higher-order upwind differencing[18] and QUICK[19] were tried for two laminar flow cases. It was found that the results were not significantly different from those obtained using hybrid differencing, indicating perhaps sufficiently fine resolution of the velocity field. In view of its relative robustness, the hybrid differencing scheme was used in all subsequent calculations.

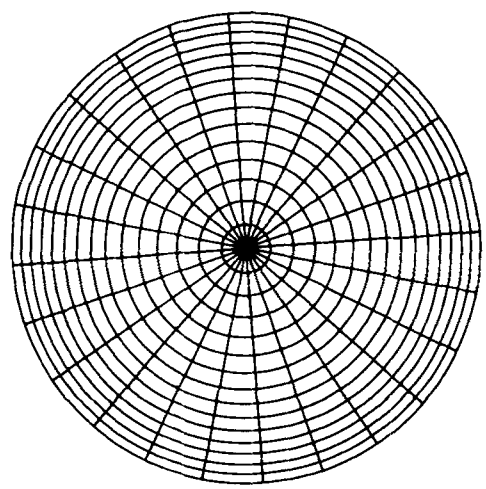

Figure 2(a). Non-uniform $r$–$\theta$ grid used for the calculation of flow in a helical coil

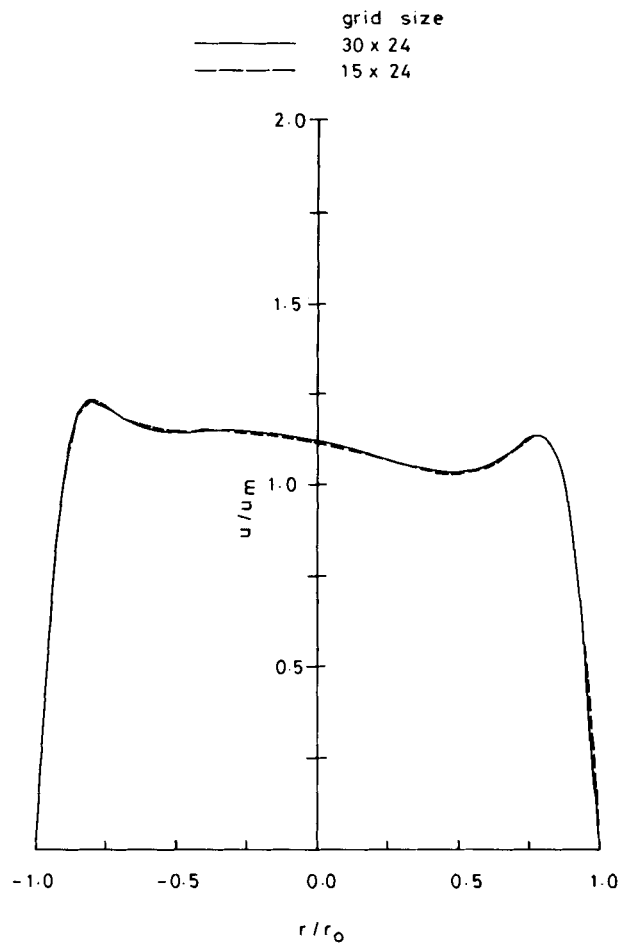


Figure 2(b). Effect of grid size on the numerical solution at a Dean number of 633. The axial velocity profiles are along a diametrical line inclined at 15° to line BB

The numerical computations were done on a $20 \times 15 \times 24$ grid in the $x$-, $r$- and $\theta$-directions respectively, with non-uniform grid spacing in the axial and radial directions. The grid in an $r$–$\theta$ plane is shown in Figure 2(a). That this grid gives sufficiently accurate results can be seen from Figure 2(b), where the axial velocity profiles obtained by a $15 \times 24$ grid and by a $30 \times 24$ grid in the fully developed flow region are compared. The grid in the axial direction was made to expand so as to have closer grid spacing in the developing region of the flow. The calculations were performed over a wide range of Dean numbers $De$, defined as $Re\sqrt{(d/D)}$, where $Re$ is the Reynolds number based on the mean flow velocity and duct inside diameter. A quantity called the total mass residual was used to test for convergence. It is defined as the sum over all control volumes of the modulus of $(\rho \mathbf{u} \cdot \mathbf{a})$ over all faces of a control volume. The solution was said to have converged if the total mass residual was less than a maximum permissible value, typically of the order of $10e^{-6}$. It was found that lower underrelaxation factors of the linear equation solvers were sometimes required to obtain convergence, especially at high Reynolds numbers.

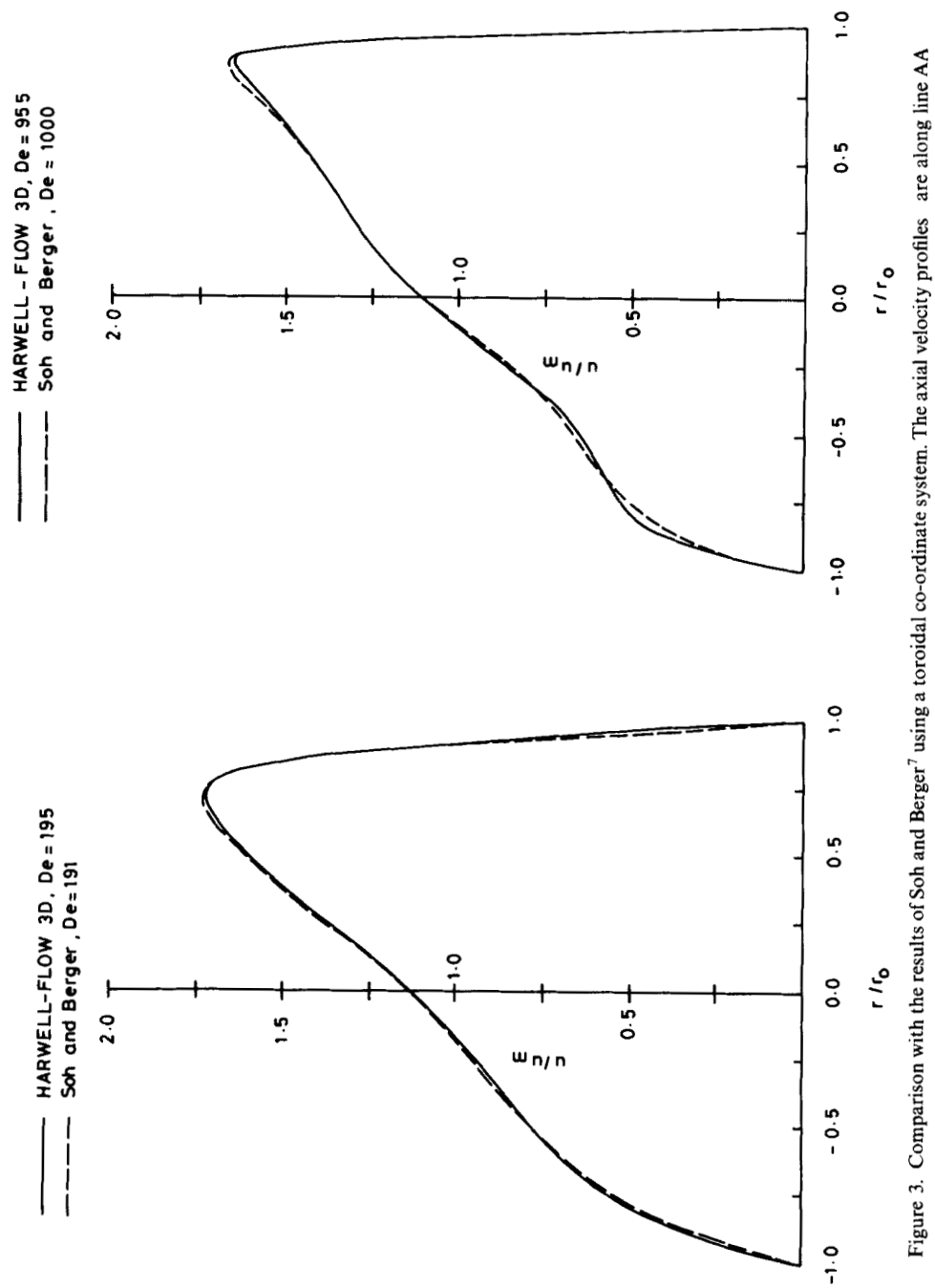


Figure 3. Comparison with the results of Soh and Berger[7] using a toroidal co-ordinate system. The axial velocity profiles are along line AA

## 4. RESULTS AND DISCUSSION

The results of our study are presented in two parts. In Section 4.1 the above model is validated for large coil-to-tube diameter ratios by qualitative and quantitative comparison with other numerical and experimental results. As discussed earlier, the model neglects terms of the order of $d/D$ and higher. The effect of these terms on the prediction of the flow field is investigated in Section 4.2.

### *4.1. Validation of model*

Flow in a helical coil is simulated by imposing a local centrifugal force on the fluid in each control volume. In order to show that this model accurately simulates the flow in a helical coil of large coil-to-tube diameter ratio, we compare the predicted flow field and temperature profiles in laminar and turbulent flow with other numerical and experimental results.

Figure 3 shows the axial velocity profile along the horizontal diametrical axis (plane AA in Figure 1) at Dean numbers of 195 and 955. Our results are compared with those of Soh and Berger,[7] who have used a toroidal co-ordinate system to solve the exact form of the Navier–Stokes equations. We find excellent agreement between the two. Figure 4 shows the

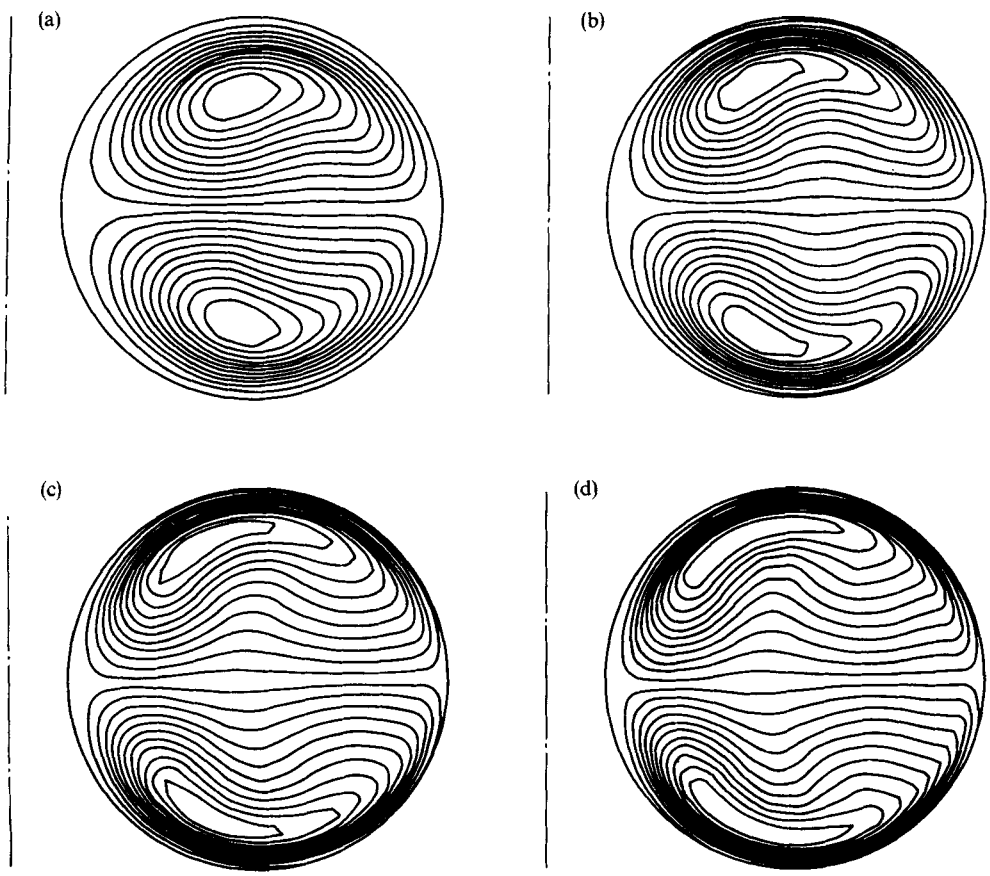


Figure 4. Streamfunction plots in an $r$–$\theta$ plane at a Dean number of (a) 195, (b) 447, (c) 633 and (d) 955. The centres of the vortices shift towards the inner side as $De$ increases

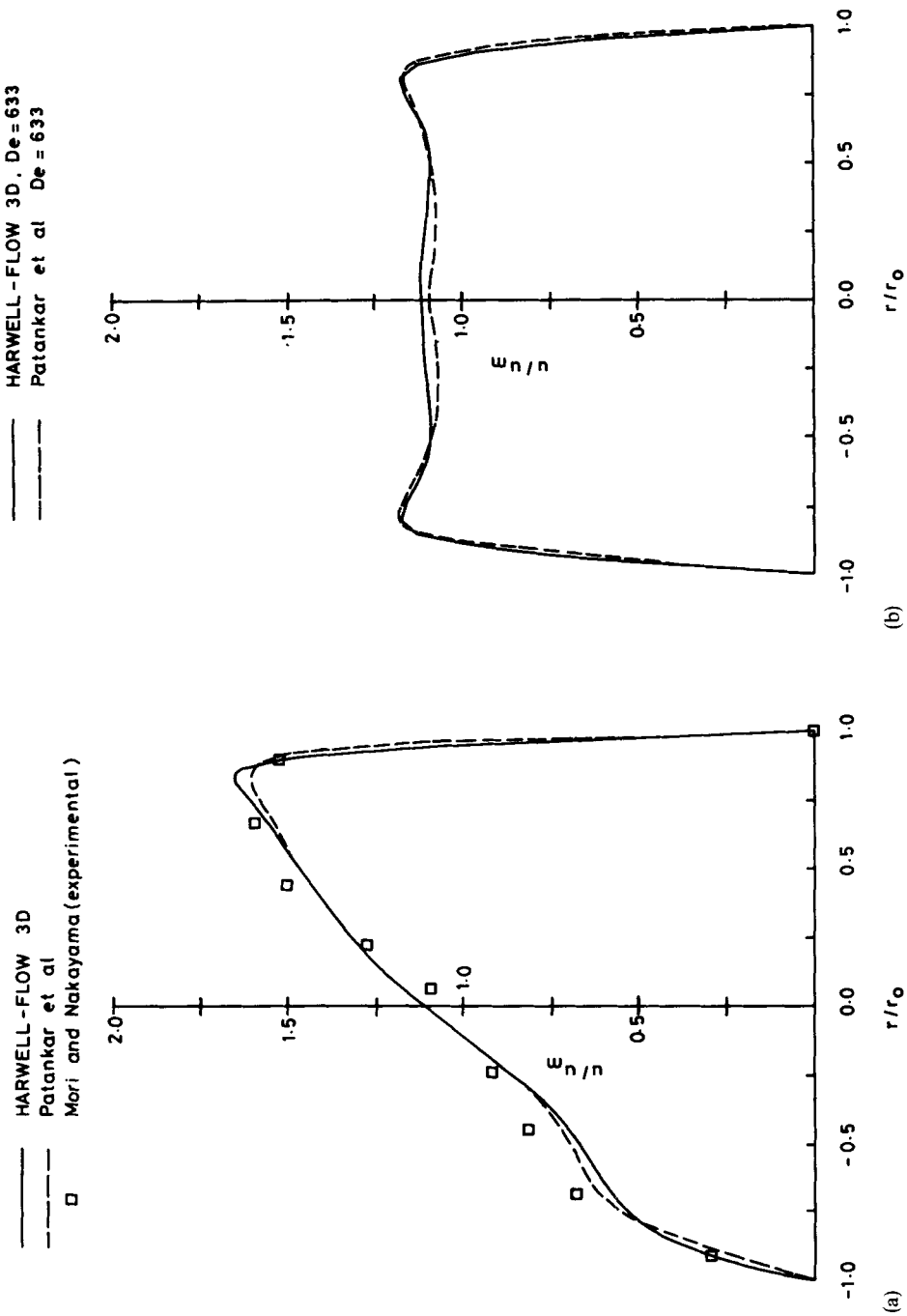


Figure 5. Comparison with the numerical results of Patankar *et al.*[6] and the experimental data of Mori and Nakayama.[2] The axial velocity profiles at Dean number of 633 are along the line AA in (a) and along BB in (b)

streamfunction contours in the fully developed flow region. We see that as the Dean number increases, the centre of the vortex shifts to the inner side of the coil, which is consistent with the interpretation of Soh and Berger.[7] Note that quantitative comparison of streamfunction contours is possible if we use the same values of velocity, diameter, density, etc. which constitute the governing non-dimensional parameters (such as *De*) of the flow. Since all this information is not available from Reference 7, the streamfunctions are only compared qualitatively. However, the fact that the velocity profiles and the friction factors agree quantitatively shows that the flow field is similar in both cases.

Figure 5 shows the comparison with the measured velocity profile of Mori and Nakayama.[2] Also shown are the predicted values of Patankar *et al.*[6] who have used a marching technique to solve an approximate form of the governing partial differential equations derived by assuming constant pressure across the cross-section. Again the agreement is quite good.

As explained in Section 2, the addition of the source $F_c$ in the momentum equations introduces certain extra terms in the $k$- and $\varepsilon$-equations. Figure 6 shows the comparison of the predicted axial velocity profile with the experimental data of Hogg.[20]. It can be seen that when the extra

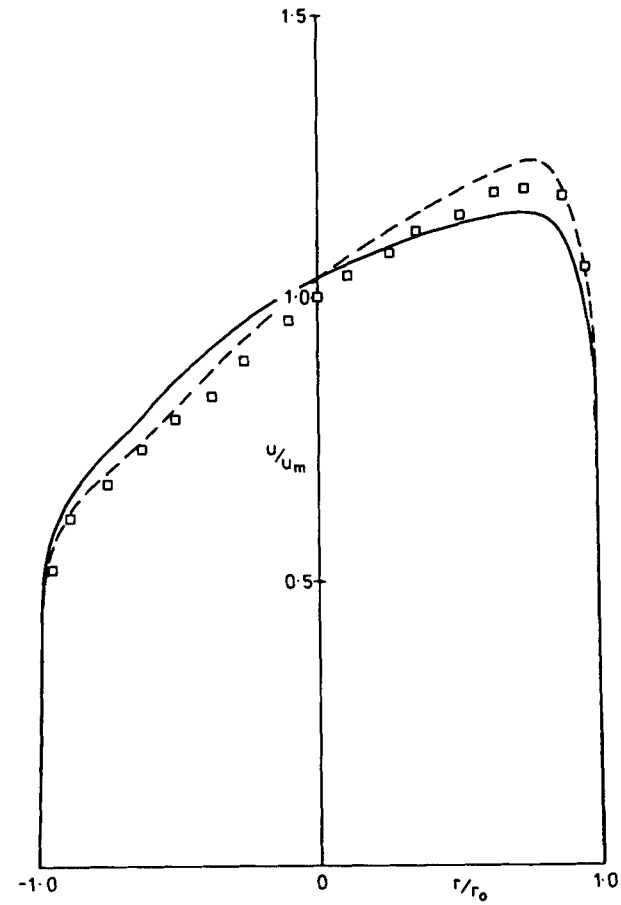


Figure 6. Comparison of the predicted axial velocity profile with experimental data in turbulent flow; $Re = 89\,000$, $D/d = 25{\cdot}9$. FLOW3D predictions with (broken line) and without (solid line) extra terms due to $F_c$ in the $k$-equation are shown. The squares represent the data of Hogg[20]

terms are included, the predicted velocity profile compares better with the measured one. The predicted friction factor also increases by about 5%, thus reducing the underprediction of the friction factor from 10% to 5% for this flow condition.

Figure 7(a) shows the predicted and the measured non-dimensionalized temperature profiles. The agreement is less satisfactory than that for the velocity profiles. This may be attributed in part to the specification of the thermal boundary conditions. In our simulations we have imposed either constant wall temperature or constant heat flux at the wall, whereas in actual experiment the heat transfer near the wall is governed by both conduction within the wall and convection in the flow. It is interesting to note that Mori and Nakayama[2] have reported nearly constant wall temperature in spite of imposing constant wall heat flux. The problem is also compounded by the distortion of the wall due to coiling, although this should have only a small effect in this case, the coil-to-tube diameter ratio being very large. It should also be noted that the numerical predictions of Patankar *et al.*[6] also fail to reproduce the experimental data and that they cite

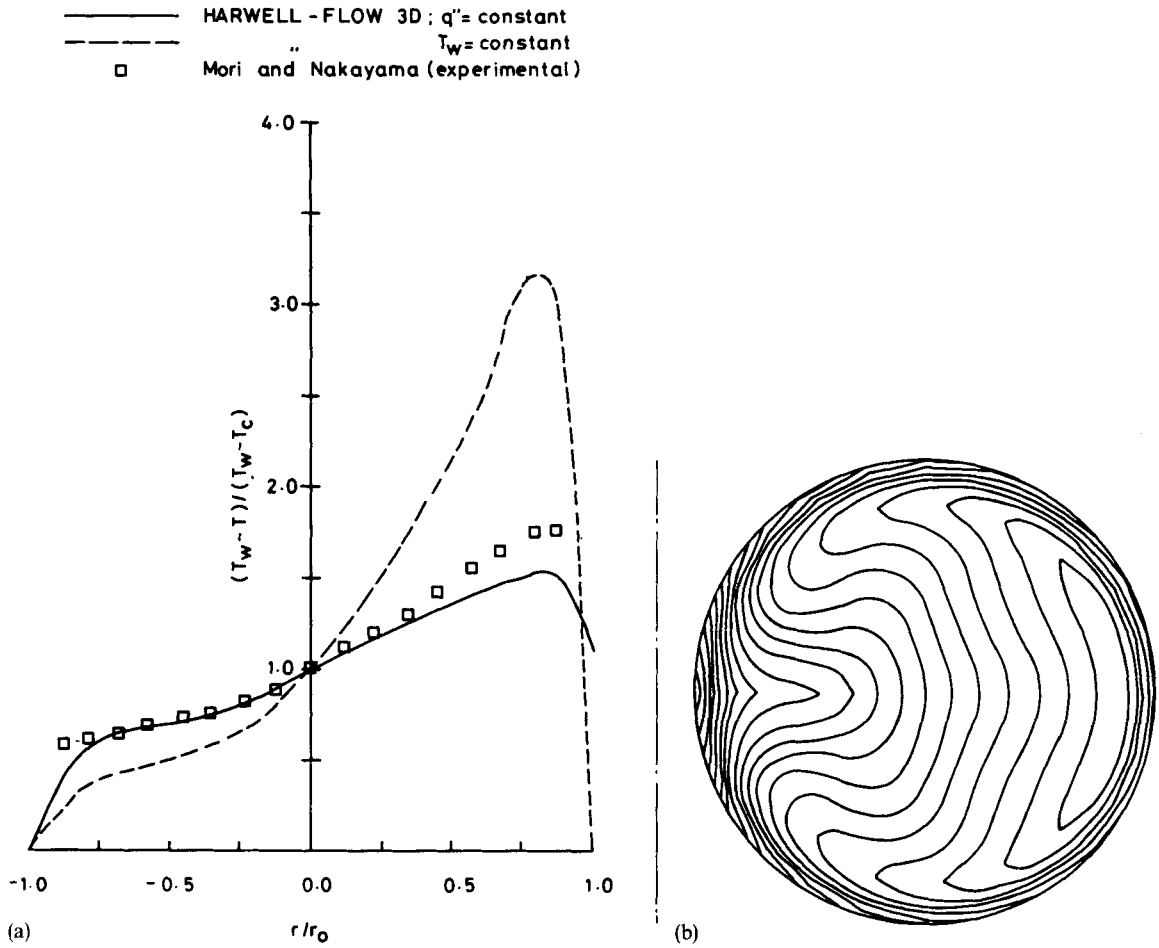


Figure 7. (a) Comparison of the predicted temperature profile with the measured data of Mori and Nakayama;[2] $Re = 4000$, $D/d = 40$ (b) Predicted temperature contours

experimental error or imperfect specification of boundary conditions in Reference 2 as possible causes. Figure 7(b) shows the predicted temperature contours in an $r$–$\theta$ plane. We note that the contours are symmetric about the horizontal plane and that the maximum wall temperature occurs on the inner wall.

Figure 8 shows the effect of buoyancy. Because of the circumferential variation of the axial velocity profile (see Figure 5), the heat transfer coefficient also varies significantly around the periphery of the tube. Thus, in a non-isothermal flow with constant wall heat flux, the average fluid temperature will be higher on the inner side of the tube (see Figure 1), where the heat transfer coefficient is low, than on the outer side. Thus the buoyancy forces will not exhibit symmetry about a vertical or a horizontal plane. The secondary flow, now a result of centrifugal force and buoyancy-driven gravitational flow, will not be symmetric either. This is reflected in Figure 8(c). The contours of temperature in buoyant flow are shown in Figure 8(d). It can be seen that the symmetry about line AA (see Figure 7(b)) is now lost and that the point of maximum wall temperature shifts upwards, although it still lies on the inner side. Our calculations show that the effect of buoyancy is pronounced only at low *De* numbers (for a given wall heat flux) and that it is negligible for the case shown in Figure 7. Thus the discrepancy between the predicted and the measured temperature profiles cannot be explained by the effect of buoyancy alone.

The coil-to-tube diameter ratio $D/d$ in the above calculations was varied between 10 and 80. The results show that the straight-tube model for simulating flow in a helical coil is valid for this range of ratios. One therefore expects the model to give satisfactory results for $D/d > 10$.

### *4.2. Application of the model to sharp bends*

The above model can be applied to advantage in the calculation of flow field in bends by imposing centrifugal force in the region of the bend. However, since bends are generally sharp, i.e. with small bend radius to duct diameter ratio, the neglect of geometric distortion terms in this model introduces an error. The extent of this error can be estimated by comparing its predictions with those from an exact simulation.

Figure 9 shows the two formulations of the problem of flow in a curved duct: (a) full simulation, where a grid in the form of the bend is generated using a boundary-fitted co-ordinate system; (b) straight-tube formulation, where the effect of curvature is modelled by adding a centrifugal force term in the momentum equation. For facility in generating the grid, the duct was taken to be of rectangular cross-section. A $30 \times 20 \times 20$ grid in the $x$- (axial), $y$- and $z$-directions was used for both methods. The grid spacing in any $y$–$z$ plane is uniform. However, in the $x$-direction the grid spacing in the region of the bend was much less than away from it. Identical grid spacing was used along the duct centreline for both the full simulation method and the straight-tube formulation method.

Figures 10 and 11 show the comparison of the axial velocity profiles in the mid-plane predicted by the two methods for a bend radius to duct hydraulic diameter ratio $D/d_h$ of 2·3 and 5 respectively. It is seen that there is significant discrepancy in the velocity profile prediction in the first case, but that it is much less in the latter. Part of this discrepancy may be due to the non-orthogonality of the grid in the full simulation. However, a major part of the discrepancy can be attributed to the neglect of terms involving the product of $d/D$ and secondary flow velocities, both of which become appreciable for sharp bends. Figure 12 shows the prediction of wall shear stress by both methods in the first case. It can be seen that although the local shear stress prediction is subject to error, the prediction of circumference-averaged shear stress (Figure 12(d)) is quite good.

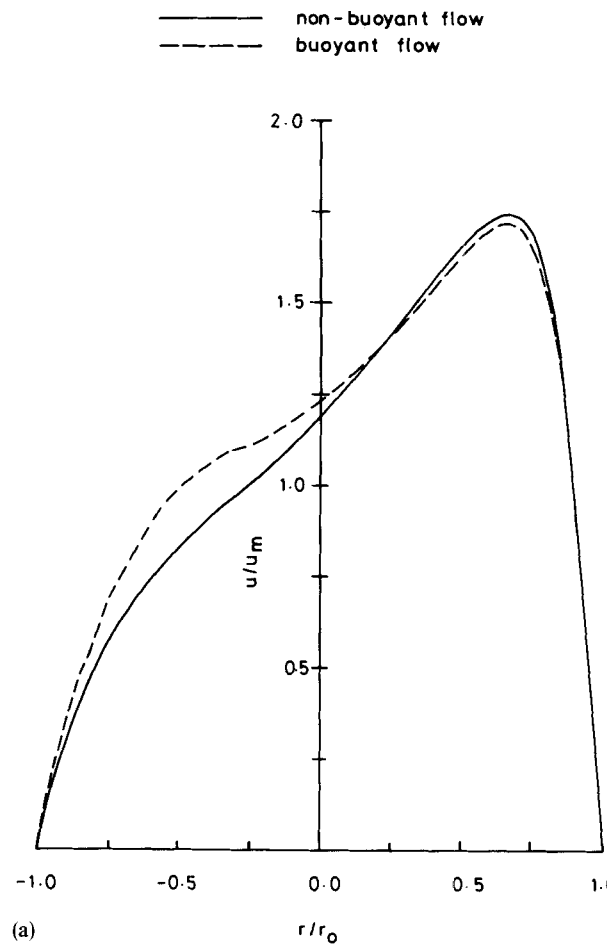


(a)

Figure 8(a)

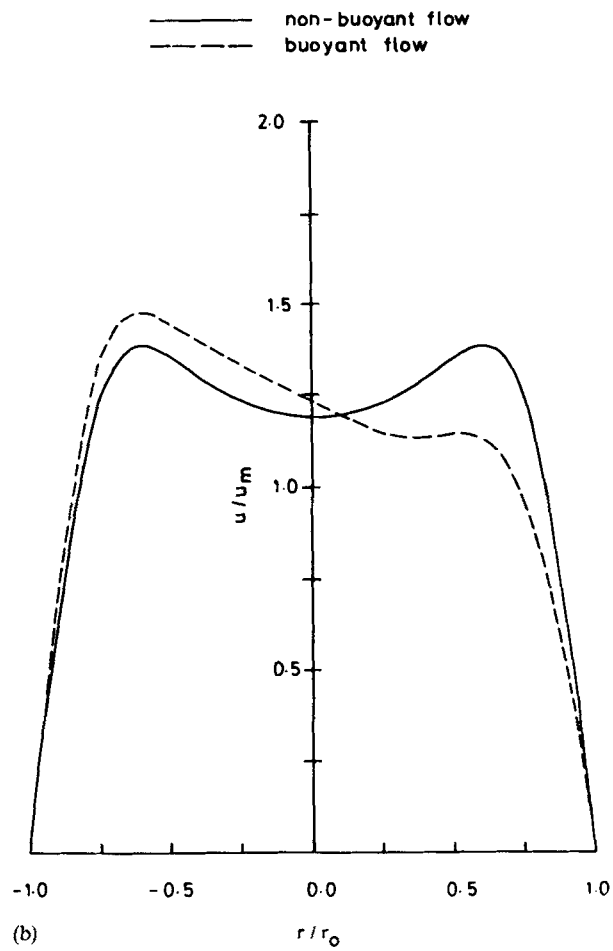


(b)

Figure 8(b)

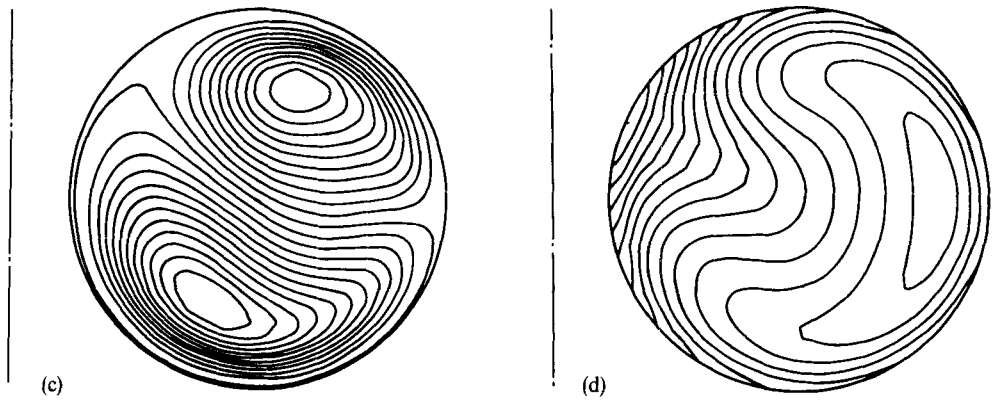


Figure 8. Effect of buoyancy at a Dean number of 138 on (a) the axial velocity profile along line AA, (b) the axial velocity profile along line BB, (c) the secondary flow in an $r$–$\theta$ plane and (d) the predicted temperature contours

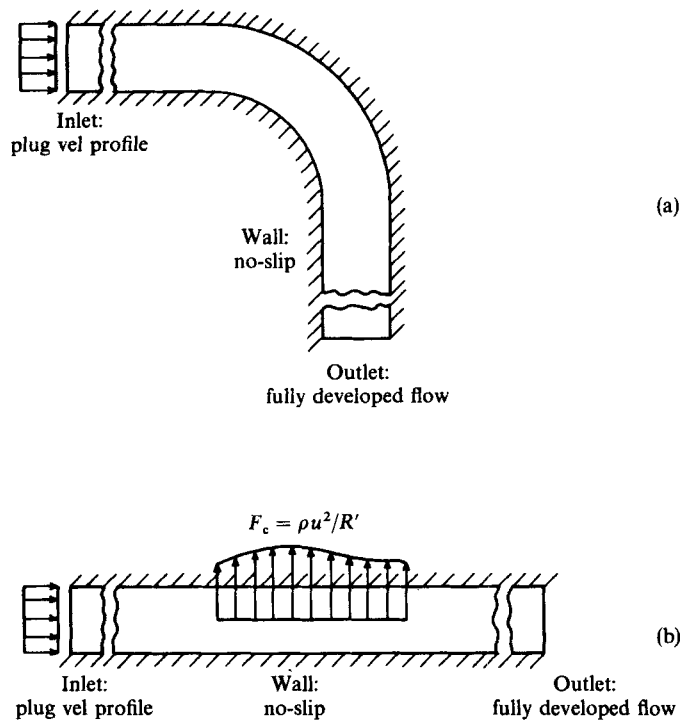


Figure 9. Two different formulations of the problem of flow in a curved duct: (a) full simulation method; (b) straight-tube method

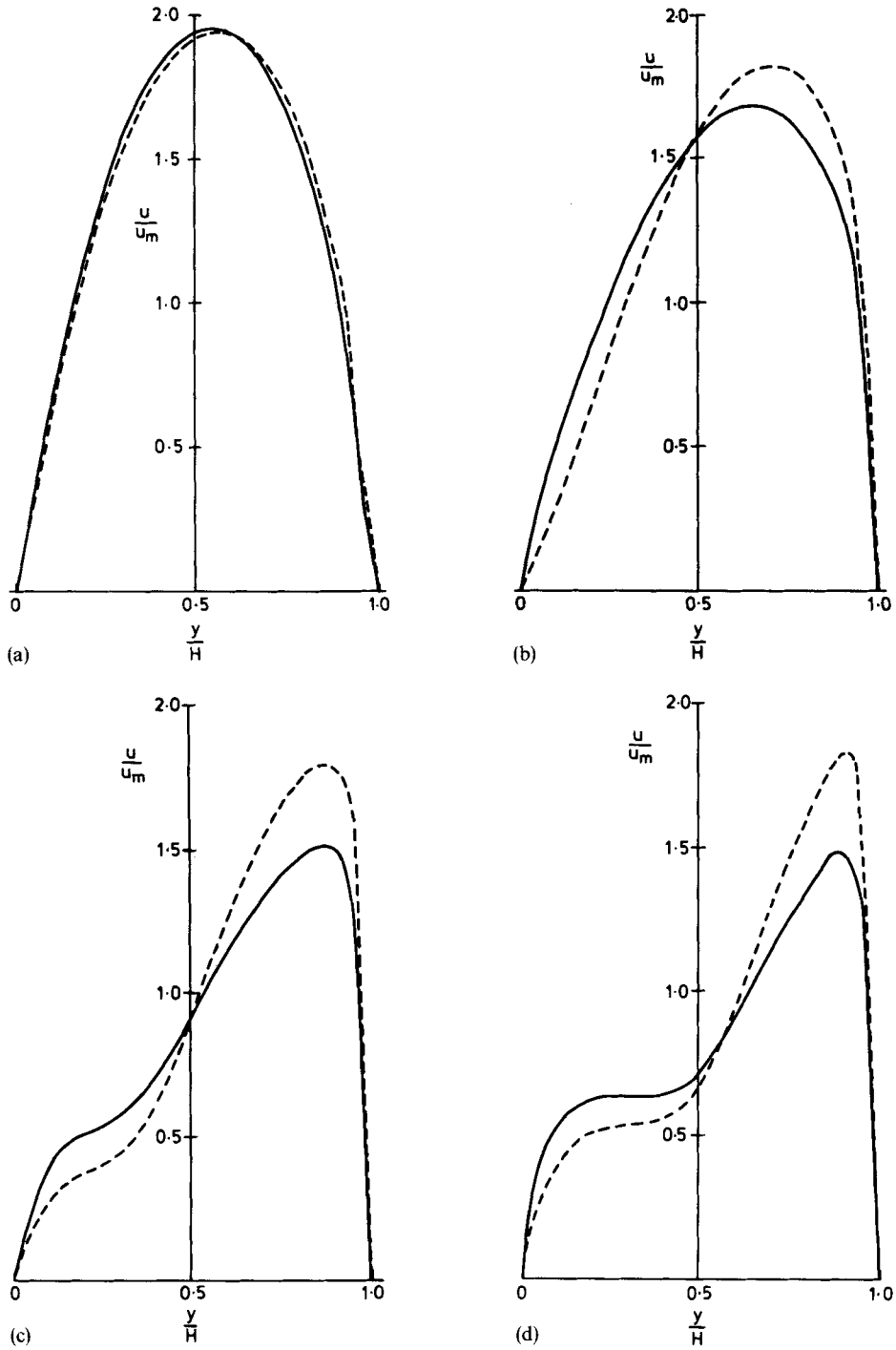


Figure 10. Comparison of the axial velocity profiles at mid-plane in a 90° bend in a duct of square cross-section. The predictions made by the full simulation method (continuous line) and by the straight-tube formulation (broken line) are compared at (a) 5°, (b) 32°, (c) 59° and (d) 86° into the bend. The Reynolds number of the flow based on the duct hydraulic diameter is 800, and the bend radius to duct diameter ratio is 2·3

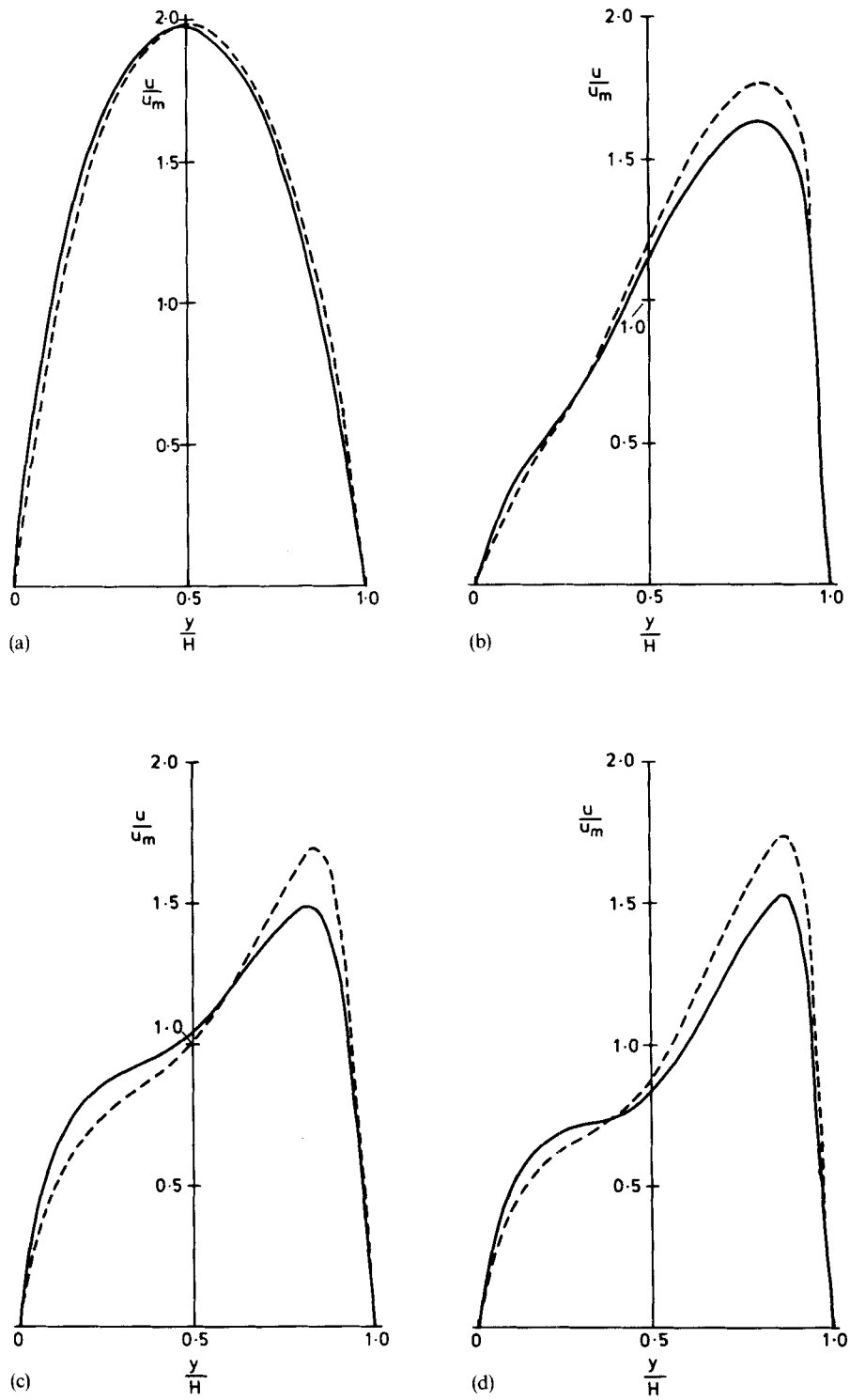


Figure 11. Same as Figure 10 except that the bend radius to duct hydraulic diameter ratio is 5

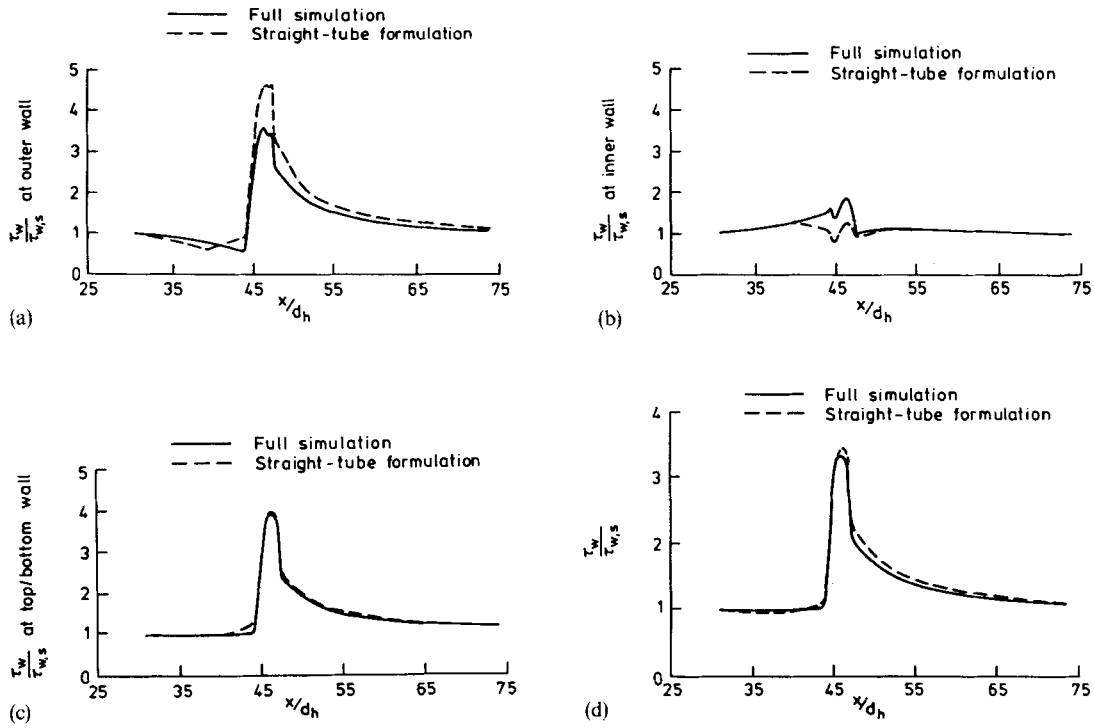


Figure 12. Comparison of the predicted wall shear stress on (a) the outer wall, (b) the inner wall, (c) the top/bottom wall and (d) the circumference-averaged value as a function of the axial distance

## 5. CONCLUSIONS

The paper describes the numerical simulation of the flow field in a curved duct by imposing a spatially varying centrifugal force on a flow in a straight tube. The model neglects certain geometric terms of the order of $d/D$ and higher. This model has been used to simulate laminar/turbulent, buoyant/isothermal flow in helical coils and bends. Comparison with experimental results and more exact numerical formulations shows that it gives excellent results for small $d/D$ ratios. For sharp bends ($d/D > 0{\cdot}2$), significant error may be expected in the prediction of local variables, although the circumference-averaged wall shear and hence the heat transfer coefficient are well predicted. In view of this, this formulation should be especially useful for engineering problems.

The straight-tube formulation should also be useful in applying advanced turbulence models such as algebraic or Reynolds stress models[13] to curved ducts. Such models are generally applicable only for an orthogonal grid. For example, they contain wall reflection terms, which are very difficult to evaluate for a non-orthogonal grid. Thus they cannot be readily applied to the simple case of flow in a curved duct of rectangular cross-section; the present formulation makes it possible to determine the flow field at least to a first approximation.

## APPENDIX I: NOTATION

| | |
|---|---|
| $\mathbf{a}$ | area vector ($m^2$) |
| $C_p$ | specific heat at constant pressure ($J\,kg^{-1}\,K^{-1}$) |
| $d$ | tube inner diameter (m) |
| $d_h$ | hydraulic diameter of the duct, (4 × flow area)/(wetted perimeter) (m) |
| $D$ | coil diameter (m) |
| $De$ | Dean number, $Re\sqrt{(d/D)}$ |
| $F_c$ | centrifugal force (N) |
| $g$ | acceleration due to gravity, 9·81 $m\,s^{-2}$ |
| $H$ | channel height (m) |
| $k$ | turbulent kinetic energy ($m^2\,s^{-2}$) |
| $p$ | pressure ($N\,m^{-2}$) |
| $q''$ | heat flux ($W\,m^{-2}$) |
| $r$ | radial position (m) |
| $r_0$ | inner radius of the tube, $d/2$ (m) |
| $R'$ | local radius of curvature (m) |
| $Re$ | Reynolds number, $u_m d/\nu$ |
| $T$ | temperature (K) |
| $T_c$ | temperature at the centre of the tube (K) |
| $T_m$ | mean temperature of the fluid (K) |
| $T_{ref}$ | reference temperature (K) |
| $T_w$ | wall temperature (K) |
| $\mathbf{u}$ | velocity vector ($m\,s^{-1}$) |
| $u_m$ | mean flow velocity of the fluid ($m\,s^{-1}$) |
| $u, v, w$ | velocity components in an orthogonal co-ordinate system |
| $x, y, z$ | Cartesian co-ordinate system |
| $x, r, \theta$ | cylindrical co-ordinate system |
| $r, \theta, \phi$ | toroidal co-ordinate system |

*Greek letters*

| | |
|---|---|
| $\beta$ | coefficient of thermal expansion ($K^{-1}$) |
| $\varepsilon$ | turbulent energy, dissipation rate ($m^2\,s^{-3}$) |
| $\lambda$ | thermal conductivity ($W\,m^{-1}\,K^{-1}$) |
| $\mu$ | dynamic viscosity ($kg\,m^{-1}\,s$) |
| $\nu$ | kinematic viscosity ($m^2\,s^{-1}$) |
| $\rho$ | density ($kg\,m^{-3}$) |
| $\rho_{ref}$ | reference density ($kg\,m^{-3}$) |
| $\tau_w$ | wall shear stress (Pa) |
| $\tau_{w,s}$ | wall shear stress in a straight duct (Pa) |

## APPENDIX II

In this paper we present a simplified 'straight-tube' formulation for the simulation of flow in a helical coil. The approximations made in this formulation can be derived by comparing it with the 'exact' formulation using a toroidal co-ordinate system.

Consider the mathematical model of Soh and Berger[7] for the fully developed flow in a helical coil. In a toroidal co-ordinate system $(r, \theta, \phi)$ the Navier–Stokes equations can be written as

axial momentum,

$$\frac{\partial u}{\partial t} + \mathbf{S}u + \frac{d}{DB}u(v\cos\theta - w\sin\theta) = \frac{1}{B} + \frac{1}{Re}\left(\mathbf{T}u - \frac{d^2}{D^2B^2}u\right);$$

radial momentum,

$$\frac{\partial v}{\partial t} + \mathbf{S}v - \frac{w^2}{r} - \frac{d\cos\theta}{DB}u^2 = \frac{\partial p}{\partial r} + \frac{1}{Re}\left[\mathbf{T}v - \frac{1}{r^2}\left(\frac{2\partial v}{\partial\theta} + w\right) - \frac{d^2\cos\theta}{D^2B^2}(v\cos\theta - w\sin\theta) + \frac{d}{DBr}w\sin\theta\right];$$

$\theta$-momentum,

$$\frac{\partial w}{\partial t} + \mathbf{S}w - \frac{vw}{r} - \frac{d\cos\theta}{DB}u^2 = -\frac{1}{r}\frac{\partial p}{\partial\theta} + \frac{1}{Re}\left[\mathbf{T}w - \frac{1}{r^2}\left(\frac{2\partial v}{\partial\theta} + w\right) - \frac{d^2}{D^2B^2}\sin\theta\,(v\cos\theta - w\sin\theta) - \frac{d}{DrB}v\sin\theta\right];$$

continuity,

$$\frac{1}{rB}\left(\frac{\partial}{\partial r}(rBv) + \frac{\partial}{\partial\theta}(Bw)\right) = 0;$$

boundary conditions, no-slip at the wall;

where

$$B = 1 + \frac{d}{D}r\cos\theta,$$

$$\mathbf{S} = \frac{1}{rB}\left(\frac{\partial}{\partial r}(rBv) + \frac{\partial}{\partial\theta}(Bw)\right),$$

$$\mathbf{T} = \frac{1}{rB}\left[\frac{\partial}{\partial r}\left(rB\frac{\partial}{\partial r}\right) + \frac{\partial}{\partial\theta}\left(\frac{B}{r}\frac{\partial}{\partial\theta}\right)\right].$$

The Reynolds number $Re$ is defined on the basis of tube radius:

$$u_0 = \left[\frac{1}{\rho}\frac{d}{D}\left(\frac{\partial p}{\partial\phi}\right)\right]^{1/2}.$$

For coils of small tube-to-coil diameter ratios, $d/D \ll 1$ and consequently

$$B = 1 + \frac{d}{D}r\cos\theta \sim 1,$$

$$\mathbf{S} = \frac{1}{r}\frac{\partial}{\partial r}(rv) + \frac{1}{r}\frac{\partial}{\partial\theta}(w),$$

$$\mathbf{T} = \frac{1}{r}\frac{\partial}{\partial r}\left(r\frac{\partial}{\partial r}\right) + \frac{1}{r}\frac{\partial}{\partial\theta}\left(\frac{1}{r}\frac{\partial}{\partial\theta}\right).$$

Thus the governing set of equations reduces to the Navier–Stokes equations in a cylindrical co-ordinate system in which an extra 'centrifugal force term' $\rho u^2/R$ is added to the appropriate momentum equations. This is our 'straight-tube' formulation.

## APPENDIX III

The addition of the centrifugal force term $F_c = \rho u^2/R'$ in the momentum equations (3) and (4) of Section 2 will introduce extra terms in the time-averaged equations for the simulation of turbulent flow. In this appendix these terms are derived and are modelled in a manner consistent with the $k$–$\varepsilon$ model.[13]

*Extra terms in the momentum equations*

Substituting $u = \bar{u} + u'$, where $\bar{u}$ is the time-averaged quantity and $u'$ is the fluctuating component in $F_c$, and taking the time average, we get

$$F_{c,t} = \text{time-averaged centrifugal force term in turbulent flow} = \frac{\rho \bar{u}^2}{R'} + \frac{\rho \overline{u'^2}}{R'}.$$

Now, since $(\overline{u'^2}/\bar{u}^2) \sim 10^{-2}$–$10^{-3}$, the contribution of the fluctuating component can be neglected. Alternatively, for isotropic turbulence, an assumption inherent in the $k$–$\varepsilon$ model,

$$\overline{u'^2} = \tfrac{4}{3}k.$$

Thus the centrifugal force term $F_c$ for turbulent flow is

$$\frac{\rho \bar{u}^2}{R'} + \frac{4}{3}\frac{\rho k}{R'}$$

and is resolved along the radial and circumferential directions.

*Extra terms in the turbulent kinetic energy equation*

The turbulent kinetic energy equation can be derived as follows. The time-averaged momentum equations are subtracted from the time-dependent ones. The resultant equation in each co-ordinate direction is multiplied by its fluctuating component of the velocity. The three equations are then summed and time-averaged. After some algebraic manipulation, the exact turbulent kinetic energy equation corresponding to the momentum equations of Section 2 can be written in a mixed tensorial and cylindrical co-ordinate system as

$$\frac{\partial k}{\partial t} + \bar{u}_i \frac{\partial k}{\partial x_i} = -\frac{\partial}{\partial x_i}\left[\overline{u_i'\left(\frac{u_j'u_j'}{2} + \frac{p}{\rho}\right)}\right] - \overline{u_i'u_j'}\frac{\partial \bar{u}_i}{\partial x_j} - \nu\overline{\frac{\partial u_i'}{\partial x_j}\frac{\partial u_j'}{\partial x_i}} + S_{F_c},$$

where

$$S_{F_c} = \text{source terms due to the centrifugal force term } F_c,$$

$$= \frac{\rho}{R'}\left[(2\bar{u}\,\overline{u'v'} + \overline{u'u'v'})\cos\theta - (2\bar{u}\,\overline{u'w'} + \overline{u'u'w'})\sin\theta\right].$$

In the above terms it can be shown that $|\overline{u'u'v'}| \ll |2\bar{u}\,\overline{u'v'}|$.

If one assumes perfect correlation between $\bar{u}'$ and $\overline{u'v'}$, then

$$|\overline{u'u'v'}| = |\sqrt{(\overline{u'^2})}|\,|\overline{u'v'}|;$$

thus

$$|\overline{u'u'v'}| \leqslant |\sqrt{(\overline{u'^2})}|\,|\overline{u'v'}|.$$

Then

$$\frac{|\overline{u'u'v'}|}{|2\bar{u}\,\overline{u'v'}|} \leqslant \left|\frac{\sqrt{(\overline{u'^2})}}{2\bar{u}}\right| \ll 1$$

and the triple correlation term can be neglected.

Thus the extra terms due to $F_c$ in the $k$-equation can be written as

$$S_{F_c} = \frac{2\rho\bar{u}}{R'}(\overline{u'v'}\cos\theta - \overline{u'w'}\sin\theta).$$

## REFERENCES


1. W. R. Dean, 'The streamline motion of fluid in a curved pipe', *Phil. Mag.*, **5**, 673–695 (1928).
2. Y. Mori and W. Nakayama, 'Study on forced convective heat transfer in curved pipe (1st report, laminar region)', *Int. J. Heat Mass Transfer*, **8**, 67–82 (1965).
3. H. Ito, 'Friction factors for turbulent flow in curved pipes', *J. Basic Eng.*, **81**, 123–134 (1959).
4. A. N. Dravid, K. A. Smith, E. W. Merril and P. L. T. Brian, 'Effect of secondary motion on laminar flow heat transfer in helically coiled tubes', *AIChE J.*, **17**, 1114–1122 (1971).
5. C. E. Kalb and J. D. Seader, 'Heat and mass transfer phenomena for viscous flow in curved circular tubes', *Int. J. Heat Mass Transfer*, **15**, 801–817 (1972).
6. S. V. Patankar, V. S. Pratap and D. B. Spalding, 'Prediction of laminar flow and heat transfer in helically coiled tubes', *J. Fluid Mech., Part 3*, **62**, 539–551 (1974).
7. W. Y. Soh and S. A. Berger, 'Fully developed flow in a curved pipe of arbitrary curvature ratio', *Int. j. numer. methods fluids*, **7**, 733–755 (1987).
8. N. Padmanabhan, 'Entry flow in heated curved pipes', *Int. J. Heat Mass Transfer*, **30**, 1453–1463 (1987).
9. K. Fugagomi and Y. Aoyama, 'Laminar heat transfer in a helically coiled tube', *Int. J. Heat Mass Transfer*, **31**, 387–396 (1988).
10. P. H. M. Bovendeerd, A. A. van Steenhoven, F. N. van Vosse and G. Vossers, 'Steady entry flow in a curved tube', *J. Fluid Mech.*, **177**, 233–246 (1987).
11. I. Dmirdzic, A. D. Gosman, R. I. Issa and M. Peric, 'A calculation procedure for turbulent flow in complex geometries', *Comput. Fluids*, **15**, 251–273 (1987).
12. A. D. Burns, N. S. Wilkes, I. P. Jones and J. R. Kightley, 'FLOW3D: body-fitted coordinates', *AERE Report-12262*, HMSO London, 1986.
13. W. Rodi, *Turbulence Models and Their Application in Hydraulics—A State-of-the-Art Review*, 2nd revised edition, University of Karlsruhe, 1984.
14. A. S. Monin and A. M. Yaglom, Statistical Fluid Mechanics, Vol. I, The MIT Press, Cambridge, MA, 1977.
15. C. M. Rhie and W. L. Chow, 'Numerical study of the turbulent flow past an airfoil with trailing edge separation', *AIAA J.*, **21**, 1527–1532 (1983).
16. J. P. van Doormaal and G. D. Raithby, 'Enhancements of the SIMPLE method for predicting incompressible fluid flows', *Numer. Heat Transfer*, **7**, 147–163 (1984).
17. R. I. Issa, 'Solution of the implicitly discretised fluid flow equations by operator splitting', *J. Comput. Phys.*, **61**, 40 (1985).
18. N. S. Wilkes and C. P. Thompson, 'An evaluation of higher-order upwind differencing for elliptic flow problems', in C. Taylor, J. A. Johnson and W. R. Smith (eds), *Numerical Methods in Laminar and Turbulent Flow*, Pineridge Press, Swansea, 1983, pp. 248–257.
19. B. P. Leonard, 'A stable and accurate convective modelling procedure based on quadratic upstream interpolation', *Comput. Methods Appl. Mech. Eng.*, **19**, 59–98 (1979).
20. G. W. Hogg, 'The effect of secondary flow on point heat transfer coefficients for turbulent flow inside curved tubes', *Ph.D. Thesis*, University of Idaho, 1968.